Explosive increase in convective Extreme El Niño events in the CO_2 removal scenario

Gayan Pathirana
POSTECH
Ji-Hoon Oh
Pohang University of Science and Technology https://orcid.org/0000-0001-8484-8997
Wenju Cai
CSIRO Oceans and Atmosphere https://orcid.org/0000-0001-6520-0829
Soon-Il An
Yonsei University https://orcid.org/0000-0002-0003-429X
Seung-Ki Min
Pohang University of Science and Technology https://orcid.org/0000-0002-6749-010X
Seo-Young Jo
POSTECH
Jongsoo Shin
Yonsei University https://orcid.org/0000-0002-3199-7646
Jong-Seong Kug (jskug@postech.ac.kr)
POSTECH https://orcid.org/0000-0003-2251-2579

Article

Keywords:

Posted Date: August 12th, 2022

DOI: https://doi.org/10.21203/rs.3.rs-1938270/v1

Abstract

Convective extreme El Niño (CEE) events, characterized by strong convective events in the eastern Pacific[1-2], are known to have a direct link to anomalous climate conditions worldwide[3-5], and it has been reported that CEE will occur more frequently under greenhouse warming[1,6-7]. Here, using a set of CO_2 ramp-up and –down ensemble experiments, we show that frequency and maximum intensity of CEE events increase further in the ramp-down period from the ramp-up period. Such changes in CEE are associated with the southward shift of the Intertropical Convergence Zone and intensified nonlinear rainfall response to SST change in the ramp-down period. The increasing frequency of CEE has substantial impacts on regional abnormal events and contributed considerably to regional mean climate changes to the CO_2 forcings.

Full Text

The unprecedented rate of global warming has raised the concern that some climate components may exceed certain thresholds, asserting irreversibility and hysteresis of the earth's climate system even if the greenhouse gases are subsequently reduced[8-10]. This issue has been intensively examined using climate models with transient CO_2 reversibility experiments[11-14], which show that the global mean temperature and precipitation respond to accumulated greenhouse gases are largely reversible within a certain period[15]. However, the path of returning to the original state (preindustrial-like climate) is thought to be not as simple as reducing greenhouse gases from the atmosphere[13]. Significant hysteresis behaviors of the climate system such as the intertropical convergence zone (ITCZ) may lead to diverse regional climate states, such as enhanced wet and dry conditions during the CO_2 decrease phase that did not occur during the increase phase[13,16]. Such hysteresis behaviors are likely resulted from a potential ocean-thermostat-related delay that masks the CO_2-driven changes. Moreover, studies revealed that the decrease in temperature lags CO_2 concentration during the ramp-down period[17-18], which induces hysteresis states with the same CO_2 level but different temperature responses, followed by different mean precipitation[19-20]. Thus, knowledge of hysteresis of certain components of the climate system is essential for preparing disaster mitigation policies[16].

El Niño/Southern Oscillation (ENSO) is a key driver of global climate variability with destructive environmental and socio-economic impacts[21-23]. The three most extreme El Niño events in 1982/83, 1997/98, and 2015/16 were characterized by massive positive Sea Surface Temperature (SST) anomalies in the Equatorial Eastern Pacific (EEP) exceeding 3ºC[21]. This led to an equatorward shift of the ITCZ[23] and an eastward shift of the equatorial convection, allowing the establishment of deep convection over the EEP, and hence intense anomalous rainfall there[1]. This is referred to as convective extreme El Niño (CEE)[2]. This reorganization of atmospheric convection caused massive widespread disruptions altering the global weather patterns[1,21-24], destroying ecosystems[25], disturbing marine life[26-27], triggering catastrophic floods and severe droughts[21], and affecting millions of people worldwide[28-29]. Such

exacerbating impacts seek an understanding of how extreme El Niño will respond to various climate change scenarios.

So far, recent studies have shown a robust projected change in the frequency of CEE under greenhouse warming[1,6-7,30]. Though there is a robust increase in the frequency of CEE in future climate, studies have shown that the mechanism of CEE does not differ between present and future climate[1,6-7]. Nevertheless, the increased CEE frequency does not merely result from the increased climatological precipitation[1], but mainly from the enhanced probability of atmospheric deep convection in the EEP due to the faster mean-state warming in the EEP than in the surrounding regions[1,6-7]. Under greenhouse warming, the equator warms faster compared to the climatological position of the ITCZ, a weaker SST perturbation is sufficient to move the ITCZ to the Niño3 region facilitating establishment of atmospheric deep convection[1-2,6-7]. Furthermore, the slope of the SST-rainfall relation becomes steeper over the Niño3 region enhancing the precipitation sensitivity under a warmer climate[31]. Thus, CEE can occur in response to even small SST anomalies.

Changes in global precipitation patterns in response to CO_2 forcing have greater importance because of the potentially destructive impacts on humans and the environment[16]. Studies indicated that future changes in precipitation patterns, primarily over the ocean are strongly influenced by SST patterns[31-33], nevertheless, such precipitation changes will have tremendous impacts on the global hydrological cycle[16]. Particularly, the southward shift of ITCZ during the ramp-down period will potentially lead to the drying of most of the tropical lands in the northern hemisphere, while ameliorating wetter conditions in certain regions worldwide[16]. Although several studies have examined the projected changes in CEE under greenhouse warming[1-2,6-7], future changes in CEE characteristics (frequency and intensity) in response to the diverse climate change scenarios remain an important scientific question. Considering the fact that our climate system shows some irreversibility and hysteresis behaviors to a given CO_2 forcing[11-14,16], how CEE will respond to a CO_2 removal scenario is critical for assessing the regional climate change and making climate policies.

In this study, analyzing an idealized CO_2 ramp-up and -down ensemble experiment using the coupled climate model CESM1[16] (see methods) we address the following questions: how CEE will change in the CO_2 removal scenario; what physical process leads to changes in the CEE frequency and intensity; and what the regional/global impacts are due to changes in CEEs.

Explosive increase in CEE

Figure 1 shows the relationship between meridional SST gradient and Niño3 rainfall in the present climate, ramp-up, -down, and restoring periods, respectively. The meridional SST gradient is defined as the mean SST over the off-equatorial region (5º N-10º N, 150º W-90º W) minus the mean over the equatorial

region (2.5º S-2.5º N, 150º W-90º W). As reported earlier[1-2,6-7], there is a clear nonlinear relation between the two variables in the present climate, and this nonlinear relation is maintained in the other warming periods. When the meridional SST becomes weaker than a certain value (about 1ºC), the Niño3 rainfall increases dramatically with the meridional SST gradient changes. It is evident that when the meridional SST gradients are reversed, the CEE events are considerably more frequent in the ramp-down period than that in the other periods, even though the CO_2 concentrations are exactly the same. These events accompanies strong convection in Niño3 region. In addition, it seems that there is an upper limit of the Niño3 precipitation which is about 12mm/day, where the Niño3 precipitation does not increase anymore despite a further decrease in meridional SST gradient.

In order to examine the changes in CEE activity, we defined CEE events when the Niño3 rainfall is larger than 5mm/day, as in previous studies[1-2,6-7]. In the present day (PD) climate, the CEE events occur in 8% of the total years, indicating that the CEE events occur once in every 12-13 years on average. Consistent with previous findings[1,7], the frequency of CEE events (16%) doubles in the ramp-up period (Fig. 1a, b). Though the CO_2 concentration is identically doubling the present level (2×367 ppm), there exists a robust difference in the occurrences of CEE between Year 2070 and 2210 (Fig. 1b, c). It is striking that the frequency of CEE explosively increases to 34% of the total years in the ramp-down period, suggesting that the CEE will occur every 3 years on average in the ramp-down period. The frequency in the ramp-down period is 4 times more than the present climate and 2 times more than in the ramp-up period. It is also noteworthy that the CEE frequency during the restoring period is still significantly higher than in the present climate, even though the CO_2 concentration has returned to the original level, suggesting some irreversibility. We also examined other models that participated in the Carbon Dioxide Removal Model Intercomparison Project (CDRMIP)[34] (see methods) whose experimental design is similar to the present experiment and found that the frequency of CEE in the ramp-down period is distinctively higher than that in the ramp-up period[7] (Supplementary Fig. 1), suggesting that the increased frequency during the ramp-down period represents a robust behaviour pattern in the CO_2 removal scenarios.

To further elucidate changes in the frequency of CEE in the evolution of CO_2 forcing we calculated the frequency of CEE with a 31-year sliding window. As the CO_2 increases in the ramp-up period, the CEE frequency increases (Fig. 2a), consistent with the previous studies[1,6-7]. After the CO_2 concentration begins to decrease from Year 2140, the CEE frequency further increases and shows a maximum at 30 years after the CO_2 peak at Year 2170 (Fig. 2a). The peak period of the CEE frequency sustains about ~15 years and begins to decrease. Therefore, the evolution of the CEE frequency shows clear asymmetric evolution in the ramp-up and –down period, and thus hysteresis behavior. In addition, even when CO_2 forcing is reduced to the PD level, the occurrences persist at a higher value. When the model is integrated 140 years further with the PD CO_2 level, the frequency of CEE still remains larger than PD, implying potential irreversibility.

In addition to the frequency, we checked changes in the maximum intensity of CEE (green line in Fig. 2a). Each maximum intensity is obtained from the maximum DJF Niño3 precipitation with the 31-year

moving windows of 28 ensemble members (green, Fig. 2a). Consistent with the frequency, the maximum intensity of CEE continuously increases in the ramp-down period, but its peak phase is further delayed. In addition, the intensity decreases much more slowly in the ramp-down period, compared to the increasing rate in the ramp-up period. Therefore, the maximum intensity at Year 2280 is much larger than that at the present climate though the CO_2 concentration is returned to its present level. In the restoring period, the maximum intensity remains much higher than the present climate, suggesting strong hysteresis and potential irreversibility.

To understand the strong hysteresis behavior for frequency and intensity of CEE, we examined the evolution of the mean states such as Niño3 mean SST and precipitation (Fig. 2b). The SST evolution approximately follows the CO_2 changes despite differences in the peak time[16,35], which is about ~20 years from the quadrupling of CO_2 (Year 2140). Though the SST is cooling down with the reduction of CO_2, the SST in the ramp-down period is considerably higher than that in the ramp-up period. Furthermore, the evolution of mean precipitation follows that of the SST changes to a large extent, in a roughly linear manner, though the maximum precipitation appears to be ~10 years delayed compared to SST (Fig. 2b). Though the mean precipitation changes are closely related to the SST changes, the evolution of precipitation lags SST during ramp-up and -down phases. This lagged precipitation response may have arisen because of the latitudinal shift of the ITCZ. It was reported from the same model experiment[16] that the delayed Southern Ocean warming and hysteresis behavior of Atlantic Meridional Overturning Circulation (AMOC) lead to the southward shift of the ITCZ in the ramp-down period. Therefore, the mean EEP precipitation shows hysteresis behavior, which contributes to the increasing frequency and intensity of CEE. In the restoring period, as the mean SST and precipitation still remain higher value than the present climate, the CEE intensity and frequency are considerably higher than the present climate.

However, the increases in the CEE frequency and intensity cannot be solely explained by the mean precipitation changes. For example, the evolution of the mean precipitation is somewhat different from the evolution of the intensity. The precipitation variability in the Niño3 region is closely related to the precipitation sensitivity to SST changes on the interannual time scale[31]. Figure 3 shows the relations between Niño3 SST and precipitation anomalies for different periods. It is clearly seen that the precipitation responds nonlinearly to the SST anomalies, consistent with the results in Fig. 1. For example, the Niño3 negative precipitation anomalies are relatively weak for La Niña and moderate El Niño SST, but strongly positive for strong El Niño SST (Fig. 3a). Since the eastern Pacific is a region of climatological atmospheric subsidence[36-37], small positive SST anomaly cannot overcome the climatological sinking motion, so the positive precipitation response is weak. Once sufficiently strong SST anomaly forcing induces a positive precipitation response against the sinking motion, it can further intensify through a positive precipitation-low level convergence feedback[1-2,6-7,31]. As the CO_2 concentration increases, the climatological sinking motion tends to be reduced so that relatively small positive SST anomaly forcing can be sufficient in inducing an eastern Pacific precipitation[1,31]. As shown in Fig. 3b and Supplementary Fig. 2a, the precipitation responses to a given SST anomaly become

stronger in the ramp-up period. In addition, the nonlinear responses become much stronger in the ramp-down period (Fig. 3c and Supplementary Fig. 2b) than that in the ramp-up period. In the ramp-down period, the Pacific ITCZ moves southward[16] so that the equatorial sinking motion in the eastern Pacific becomes quite weak, which leads to a stronger precipitation response to a given SST anomaly. Such strong air-sea coupling can allow CEE events to be developed to even small positive SST anomalies. In the restoring period, the nonlinear air-sea coupling is stronger than in the present climate, which contributes to more frequent and intensified CEE events (Fig. 3d and Supplementary Fig. 2c).

To clearly show differences in the air-sea coupling strength between the ramp-up and –down periods, the precipitation composites of moderate El Niño events are calculated. To avoid the effect of the different El Niño magnitudes, we have selected the El Niño cases whose Niño SST is between 1ºC – 2ºC (Fig. 3e, f, and Supplementary Fig. 2d, e). It is clear that the precipitation anomalies in the ramp-down period are much greater than those in the ramp-up period. In particular, the difference is much distinctive in the EEP (Fig. 3g, and Supplementary Fig. 2f), which is closely related to the CEE. Hence, we suggest here that the strong hysteresis behavior of the frequency and intensity of CEE during the ramp-down period resulted from increased mean precipitation, and enhanced precipitation sensitivity to SST change in the EEP region.

Impacts of the frequent and intensive CEE

As the CEE precipitation leads to tremendous atmospheric circulation changes, its change has substantial impacts on the global hydrological cycle. For example, the two strongest El Niño events (i.e., 1997/98 and 2015/16) on records have shown the complex remote impacts causing drier conditions over northeast Brazil, northeast Australia, and India[38-40], and wetter conditions over California, Ecuador, northern Peru, and southern China during boreal winter[41-43]. Based on these characteristics of CEE, understanding the remote impacts of more frequent and intensive CEE during the ramp-down period would be of great regional socio-economic help associated with future climate adaptation policies. Therefore, we investigated the more frequent and intensive CEE-induced changes in land precipitation as well as the CEE teleconnection pattern change itself. First, to show the changes in the teleconnection patterns, we calculated the composite of CEE precipitation (Supplementary Fig. 3a, b) and surface air temperature (SAT) (Supplementary Fig. 4a, b) anomalies in the PD climate and the Year 2210, respectively. The results show that there is no significant difference in the patterns between the PD climate and the ramp-down phase. Second, we examined the contribution of the CEE events to the mean state by considering changes in frequency and intensity of CEE (see methods). Because the CEE is highly nonlinear phenomenon (i.e., no convective La Niña event), the CEE activity and its modulation contribute to the mean state changes. In spite of the identical CO_2 forcing, there are profound differences in the contribution to the mean-state of precipitation (Supplementary Fig. 3c, d) and SAT (Supplementary Fig. 4c, d) between the PD climate and the Year 2210. In other words, because the teleconnection pattern of CEE is almost the same (Supplementary Fig. 3-4) between the PD climate and Year 2210, more frequent

and intensive CEE events contribute more to the mean climate state of the regions where CEE impact is evident.

With the more frequent and intensive CEEs during the ramp-down period, the regions which are being influenced by the CEE will undergo profound wet and dry conditions (Fig. 4). In particular, the precipitation in the extratropical Northern and Southern America, East Asia, and tropical Africa significantly increases in the ramp-down period (Fig. 4a). In addition, there are drier conditions over tropical South America, Northwestern Australia, and South Asia. Though most of the regions with enhanced wet and dry conditions due to CEE during boreal winter are weakened in the following spring, the wetter (drier) conditions over East Asia (Northwestern Australia) are further enhanced due to distinct impacts of CEE (Fig. 4b). Note that the pattern of the CEE contribution is quite similar to the regional hysteresis pattern shown in Kug et al. 2022, suggesting that the CEE play a critical role in leading hysteresis behavior in the regional hydrological cycle.

Moreover, the increasing frequency of CEE significantly contributes to the mean SAT changes, implying enhanced warm (i.e., extratropical South America, Australia) and cold conditions (i.e., extratropical North America) in certain regions worldwide (Supplementary Fig. 5a, b). Thus, the regional climate change in lands is affected by both the increasing frequency and intensity of CEE. To further emphasize the impacts of CEE during the ramp-down phase we show the difference in total extreme precipitation days[44] (>= 20mm, see methods) during CEE events between the PD climate and the Year 2210 (Supplementary Fig. 6). The results show that the difference in total extreme precipitation days during CEE is consistent with the contribution to the mean-state change by CEE displayed in Fig. 4. For example, the number of extreme precipitation days during CEE will be further increased over extratropical Northern and Southern America, East Asia and tropical Africa in the boreal winter and spring, suggesting that these regions will experience more extreme events due to the more frequent and intensified CEE events during the ramp-down period. In addition, consistent with enhanced drier conditions, the number of extreme precipitation days will also be decreased over Northwestern Australia during CEE, implying that Australia may experience more droughts during the ramp-down period.

Discussion

In this study, we investigated the future change in frequency and intensity of CEE using an idealized CO_2 ramp-up and -down ensemble experiment with extreme CO_2 changes. We show that the CEE will be more frequent and intense during the CO_2 removal phase and such changes are associated with the southward shift of the ITCZ and enhanced non-linear precipitation response to a given SST in the EEP region. Also, we have shown some irreversibility of the frequency and intensity of CEE in the restoring period. Such irreversible behaviors arise due to the different adjustment timescales of associated climate components[16]. Further, the future changes of CEE will contribute to the mean-state changes in regional climate due to its intrinsic nonlinear characteristics. Moreover, with the projected large increase of CEE

events, the more frequent occurrence of potential devastating weather events can be anticipated in the future even though the CO_2 emissions are reduced and even negative.

The increase of CO_2 in the ramp-up period in the current experiment is comparable to the Shared Socio-economic Pathway (SSP) 5-8.5 scenario in the Coupled Model Intercomparison Project Phase 6 (CMIP6) simulation. Therefore, the projected changes in the CEEs are equivalent to those from the extreme CO_2 emission scenario, and we may not exclude the possibility that the results are sensitive to the experimental model design. To show the robustness of the CEE response, we also analyzed five model simulations from CDRMIP and found a consistent CEE response, to the results of the present experiment (Supplementary Fig. 1). The climate models simulate the nonlinear relation between the meridional SST gradient and Niño3 rainfall. Though the frequency of CEE differs among models, all the models show an increase in CEE frequency in the CO_2 removal period. Thus, in agreement with the present experiment results, the CDRMIP analysis shows a further increase in CEE frequency in the ramp-down period.

In addition, the projected increased frequency of extreme El Niño is shown to be linked to the faster warming in the EEP region[1–2,6–7,23]. However, the surface warming pattern depicted in the climate models is contrary to the observations, where the tropical SST trend over the recent decades shows a suppressed warming in the EEP region[35,45]. Therefore, understanding the model biases of the simulated warming in the EEP may be important[35] for more reliable projection of ENSO properties and associated teleconnections[21,45–46]. Nevertheless, our study provides the implication of impacts from evolving CO_2, which could be far worse than we expect, due to hysteresis/irreversible behaviors of the climate system. Thus, a climate mitigation policy must be taken into account not only for reducing the damages of immediate climate changes but also to prevent the expected irreversible changes.

References

1. Cai, W., Borlace, S., Lengaigne, M. *et al.* Increasing frequency of extreme El Niño events due to greenhouse warming. *Nat. Clim. Chang.* **4,** 111–116 (2014). https://doi.org/10.1038/nclimate2100.
2. Wang, G., Cai, W. & Santoso, A. Stronger Increase in the Frequency of Extreme Convective than Extreme Warm El Niño Events under Greenhouse Warming. *Journal of Climate,* 33(2), 675-690 (2020). https://doi.org/10.1175/JCLI-D-19-0376.1.
3. Philander, S. G. H. Anomalous El Niño of 1982-83. *Nature* **305,** 16 (1983).
4. Glynn, P. W. & de Weerdt, W. H. Elimination of two reef-building hydrocorals following the 1982-83 El Niño. *Science* **253,** 69-71 (1991).
5. Goddard, L. & Gershunov, A. Impact of El Niño on weather and climate extremes. In *El Niño Southern Oscillation in a changing climate* (eds McPhaden, M. J, Santoso, A. & Cai, W.) 361–375 (2020). https://doi.org/10.1002/9781119548164.ch16.
6. Cai, W., Wang, G., Santoso, A., Lin X. & Wu L. Definition of extreme El Niño and its impact on projected increase in extreme El Niño frequency. *Geophys. Res. Lett.* **44**, 184–190 (2017).

7. Wang, G., Cai, W., Gan, B. *et al*. Continued increase of extreme El Niño frequency long after 1.5C warming stabilization. *Nat. Clim. Chang.* **7,** 568–572 (2017). https://doi.org/10.1038/nclimate3351.
8. Lenton, T. M. *et al*. Tipping elements in the Earth's climate system. *Proc. Natl Acad. Sci. USA* **105**, 1786–1793 (2008).
9. Lenton, T. M. Early warning of climate tipping points. *Nat. Clim. Chang*. **1**, 201–209 (2011).
10. Swingedouw, D. *et al*. Early warning from space for a few key tipping points in physical, biological, and social-ecological systems. *Surv. Geophys*. **41**, 1237–1284 (2020).
11. Lowe, J. A. et al. How difficult is it to recover from dangerous levels of global warming? *Environ. Res. Lett*. **4**, 014012 (2009).
12. Gillett, N. P., Arora, V. K., Zickfeld, K., Marshall, S. J. & Merryfield, W. J. Ongoing climate change following a complete cessation of carbon dioxide emissions. *Nat. Geosci*. **4**, 83–87 (2011).
13. Chadwick, R., Wu, P., Good, P. *et al.* Asymmetries in tropical rainfall and circulation patterns in idealised CO_2 removal experiments. *Clim. Dyn.* **40,** 295–316 (2013). https://doi.org/10.1007/s00382-012-1287-2.
14. Jeltsch-Thömmes, A., Stocker, T. F. & Joos, F. Hysteresis of the Earth system under positive and negative CO 2 emissions. *Environ. Res. Lett*. **15**, 124026 (2020).
15. Wu, P., Ridley, J., Pardaens, A., Levine, R. & Lowe, J. The reversibility of CO 2 induced climate change. *Clim. Dyn*. **45**, 745–754 (2015).
16. Kug, J.-S., Oh, J-H., An, S.-I. *et al.* Hysteresis of the intertropical convergence zone to CO_2 forcing. *Nat. Clim. Chang.* **12,** 47–53 (2022). https://doi.org/10.1038/s41558-021-01211-6.
17. Boucher, O., Halloran, P.R., Burke, E.J. *et al*. Reversibility in an Earth system model in response to CO_2 concentration changes. *Env Res Lett.* **7(2),** 024013 (2012). https://doi.org/10.1088/1748-9326/7/2/024013.
18. Ehlert, D. & Zickfeld, K. Irreversible ocean thermal expansion under carbon dioxide removal. *Earth Syst Dynam.* **9,** 197-210 (2018). https://doi.org/10.5194/esd-9-197-2018.
19. Andrews, T., Forster, P. M. & Gregory, J. M. A surface energy perspective on climate change. *Journal of Climate* **22(10)**, 2557–2570 (2009).
20. Cao, L., Bala, G. & Caldeira, K. Why is there a short-term increase in global precipitation in response to diminished CO2 forcing? *Geophys Res Lett*, **38**(L06703) (2011).
21. Philander, S. G. H. Anomalous El Niño of 1982–83. *Nature* **305**, 16 (1983).
22. McPhaden, M. J., Zebiak, S. E. & Glantz, M. H. ENSO as an integrating concept in Earth science. *Science*, **314**, 1740–1745 (2006).
23. Cai, W., Santoso, A., Wang, G. *et al.* ENSO and greenhouse warming. *Nature Clim Change* **5,** 849–859 (2015). https://doi.org/10.1038/nclimate2743.
24. Power, S., Delage, F., Chung, C., Kociuba, G. & Keay, K. Robust twenty-first-century projections of El Niño and related precipitation variability. *Nature* **502**, 541–545 (2013).

25. Merlen, G. The 1982–1983 El Niño: Some of its consequences for Galapagos wildlife. *Oryx*, **18**, 210–214 (1984).
26. Aronson, R. B. et al. Coral bleach-out in Belize. *Nature*, **405**, 36 (2000).
27. Chavez, F. P., Ryan, J., Lluch-Cota, S. E. & Ñiquen, M. From anchovies to sardines and back: Multidecadal change in the Pacific Ocean. *Science*, **299**, 217–221 (2003).
28. Sponberg, K. Compendium of Climatological Impacts, University Corporation for Atmospheric Research Vol. 1 (National Oceanic and Atmospheric Administration, Office of Global Programs, 1999).
29. Rao, V.B., Maneesha, K., Sravya, P. *et al.* Future increase in extreme El Nino events under greenhouse warming increases Zika virus incidence in South America. *npj Clim Atmos Sci* **2,** 4 (2019). https://doi.org/10.1038/s41612-019-0061-0.
30. Lengaigne, M. & Vecchi, G. A. Contrasting the termination of moderate and extreme El Niño events in coupled general circulation models. *Clim. Dynam*. **35**, 299–313 (2010).
31. Yun, KS., Lee, JY., Timmermann, A. *et al.* Increasing ENSO–rainfall variability due to changes in future tropical temperature–rainfall relationship. *Commun Earth Environ* **2,** 43 (2021). https://doi.org/10.1038/s43247-021-00108-8.
32. Xie, S. P. *et al.* Global warming pattern formation: Sea surface temperature and rainfall. *J. Clim.* **23**, 966–986 (2010).
33. Johnson, N. & Xie, S.P. Changes in the sea surface temperature threshold for tropical convection. *Nature Geosci* **3,** 842–845 (2010). https://doi.org/10.1038/ngeo1008.
34. Eyring, V. *et al.* Overview of the Coupled Model Intercomparison Project Phase 6 (CMIP6) experimental design and organization. *Geosci. Model Dev*. **9**, 1937–1958 (2016).
35. Heede, U.K. & Fedorov, A.V. Eastern equatorial Pacific warming delayed by aerosols and thermostat response to CO_2 increase. *Nat. Clim. Chang.* **11,** 696–703 (2021). https://doi.org/10.1038/s41558-021-01101-x.
36. Cai, W., Wang, G., Dewitte, B. *et al.* Increased variability of eastern Pacific El Niño under greenhouse warming. *Nature* **564,** 201–206 (2018). https://doi.org/10.1038/s41586-018-0776-9.
37. Kug, J.-S., Jin, F.F. & S.-I. An. Two types of El Niño events: Cold tongue El Niño and warm pool El Niño. *J. Clim.* **22**, 1499–1515 (2009). https://doi:10.1175/2008JCLI2624.1.
38. Rodrigues, R. R., Haarsma, R. J., Campos, E. J. D. *et al*. The Impacts of Inter-El Niño Variability on the Tropical Atlantic and Northeast Brazil Climate. *J. Clim.* **24**, 3402-3422 (2011). https://doi.org/10.1175/2011JCLI3983.1.
39. Cai, W., Rensch, P. V., Cowan, T. *et al*. Asymmetry in ENSO teleconnection with regional rainfall, its multidecadal variability, and impact. *J. Clim.* **23**, 4944-4955 (2010). https://doi.org/10.1175/2010JCLI3501.1.
40. Dewitte, B. &Takahashi, K. Extreme El Niño events. *Tropical Extremes*, 165-201 (2019). https://doi.org/10.1016/B978-0-12-809248-4.00006-6.

41. Jong, B.-T., Ting, M. & Seager, R. El Niño's impact on California precipitation: seasonality, regionality, and El Nino intensity. *Environ. Res. Lett.* **11**, 054021 (2016). https://doi.org/10.1088/1748-9326/11/5/054021.
42. Chen, J., Wang, X., Zhou, W. *et al*. Unusual rainfall in Southern China in Decaying August during Extreme El Niño 2015/16: Role of the Western Indian Ocean and North Tropical Atlantic SST. *J. Clim.* **31**, 7019-7034 (2018). https://doi.org/10.1175/JCLI-D-17-0827.1.
43. Sun, X., Renard, B., Thyer, M. *et al*. A global analysis of the asymmetric effect of ENSO on extreme precipitation. *Journal of Hydrology* **530**, 51-65 (2015). https://doi.org/10.1016/j.jhydrol.2015.09.016.
44. Zhang, X., Alexander, L., Hegerl, G. C. *et al*. Indices for monitoring changes in extremes based on daily temperature and precipitation data. *WIRESs Climate Change* **2(6)**, 851-870 (2011). https://doi.org/10.1002/wcc.147.
45. Li, G. & Xie, S.-P. Tropical biases in CMIP5 multimodel ensemble: The excessive equatorial Pacific cold tongue and double ITCZ problems. *J. Clim.* **27**, 1756-1780 (2014).
46. Lopez, H., Lee, S.K., Kim, D. *et al*. Projections of faster onset and slower decay of El Niño in the 21st century. *Nat. Commun.* **13,** 1915 (2022). https://doi.org/10.1038/s41467-022-29519-7.

Methods

Dataset: to examine the occurrences of CEE events to CO_2 forcing, data from idealized CO_2 ramp-up and ramp-down experiment has been used[16,47]. The model used in the present study is a fully-coupled Community Earth System Model version 1.2.2, which has the same component models and coupling of the CESM1 with the Community Atmosphere Model version 5 (CAM5) in CMIP5. The experiment consists of two simulations. One is present-day run (PD) with a constant CO_2 concentration (367 ppm) over 900 years. The second is a CO_2 ramp-up and -down experiment based on 28 initial conditions extracted from the PD. Here, atmospheric CO_2 concentration is set to increase at a rate of 1% per year over 140 years until CO_2 quadrupling up to 1468 ppm (ramp-up), and then a decreasing CO_2 forcing at the same rate over 140 years until it reaches to the PD value of 367 ppm (ramp-down). Here, the increasing CO_2 concentration in the ram-up period is comparable with the SSP 5-8.5 Scenario in the CMIP6 simulation[48]. Further, a restoring run has been conducted for 220 years with a constant CO_2 concentration of 367 ppm.

In addition, we analyze the five CMIP6[34] models (ACCESS-ESM1-5, CanESM5, CESM2, MIROC-ES2L, UKESM1-0-LL) with 1pctCO2 gradual CO_2 rise and the 1pctCO2-cdr scenarios from the Carbon Dioxide Removal Model Intercomparison Project (CDRMIP)[49], where CO_2 increases are relative to a pre-industrial level of 284.7 ppm. The experimental setup is corresponding to our experiment, except for the initial CO_2 level. However, the increasing frequency of CEE calculated from CMIP6 is quite consistent with the results of our experiment.

Further, to show the changes in extreme precipitation days during CEE events in CO_2 removal period we analyze the number of rainy days that exceed the threshold of 20mm/day[44]. First, we calculate the

extreme precipitation days anomaly (seasonal climatology has been removed) in boreal winter and the following spring. Next, we take the cumulative summation of the total anomalous extreme precipitation days during CEE in Year 2210 (28 ensembles and 31-year window) and PD climate (1 ensemble and 900-year window). Then we display the mean (ensemble and time) difference (Year 2210 minus PD) of anomalous extreme precipitation days (Supplementary Fig. 6) to exhibit the regions that will suffer from CEE during decarbonization. To display the distinct changes, the values are multiplied by 31, and therefore, the unit given in Supplementary Fig. 6 is total extreme precipitation days per 31-years.

Definition of CEE index: boreal winter (December-January-February) total rainfall larger than the threshold value of 5mm/day in the eastern equatorial Pacific (Niño3 region: 5º S-5º N, 150º W-90º W) is used to define a convective extreme El Niño event[1-2,6-7].

Metrics: the meridional SST gradient has been defined as the average SST over the off-equatorial region (5º N-10º N, 150º W-90º W) minus the average over the equatorial region (2.5º S-2.5º N, 150º W-90º W)[1].

The DJF rainfall rate curves in Fig. 3 were calculated using the detrended Niño3 rainfall anomalies corresponding to Niño3 SST anomalies binned at 0.5º C. The changes in the land precipitation shown in Fig. 4 is calculated as the contribution to the mean-state change by CEE in Year 2210 (Supplementary Fig. 3d) minus the contribution to the mean-state change by CEE in PD climate (Supplementary Fig. 3c). The changes in SAT shown in Supplementary Fig. 5 is calculated similar to that of Fig. 4. Contribution to the mean-state (i.e., Supplementary Fig. 3d) is calculated as the sum of precipitation anomalies of total CEE events (i.e., 289 CEE events during 2195 to 2225) divided by the total ensemble years in each period (i.e., 28 ensembles x 31 years).

References

47. Kug, J.-S. *et al*. Data for hysteresis of the intertropical convergence zone to CO2 forcing. *Figshare* https://doi.org/10.6084/m9.figshare.16669324 (2021).
48. Meinshausen, M. *et al*. The shared Socio-economic Pathway (SSP) greenhouse gas concentrations and their extensions to 2500. *Geosci. Model Dev.* **13,** 3571–3605 (2020).

49. Keller, D. P. *et al*. The Carbon Dioxide Removal Model Intercomparison Project (CDRMIP): rationale and experimental protocol for CMIP6. *Geosci. Model Dev.* **11,** 1133–1160 (2018).

Declarations

Data availability

The data used in the study are available at https://doi.org/10.6084/m9.figshare.16669324. CMIP6 data are available at https://esgf-node.llnl.gov/projects/cmip6/. Climate indices are available at https://www.climdex.org.

Code availability

All plots and analyses are carried out using Python v. 3.9 including supportive packages. The code used in this study is available from the corresponding author upon reasonable request.

Acknowledgments

This work was supported by the National Research Foundation of Korea (NRF-2022R1A3B1077622, NRF-2018R1A5A1024958). The CESM simulation was carried out on the supercomputer supported by the National Center for Meteorological Supercomputer of Korea Meteorological Administration (KMA), the National Supercomputing Center with supercomputing resources, associated technical support (KSC-2021-CHA-0030), and the Korea Research NETwork (KREONET).

Author contributions

G.P. conducted analysis, prepared the figures and wrote the manuscript. J.-S.K. designed the research and wrote the majority of the manuscript content. All of the authors discussed the study results and reviewed the manuscript.

Competing interests

Authors declare no competing interests

Figures

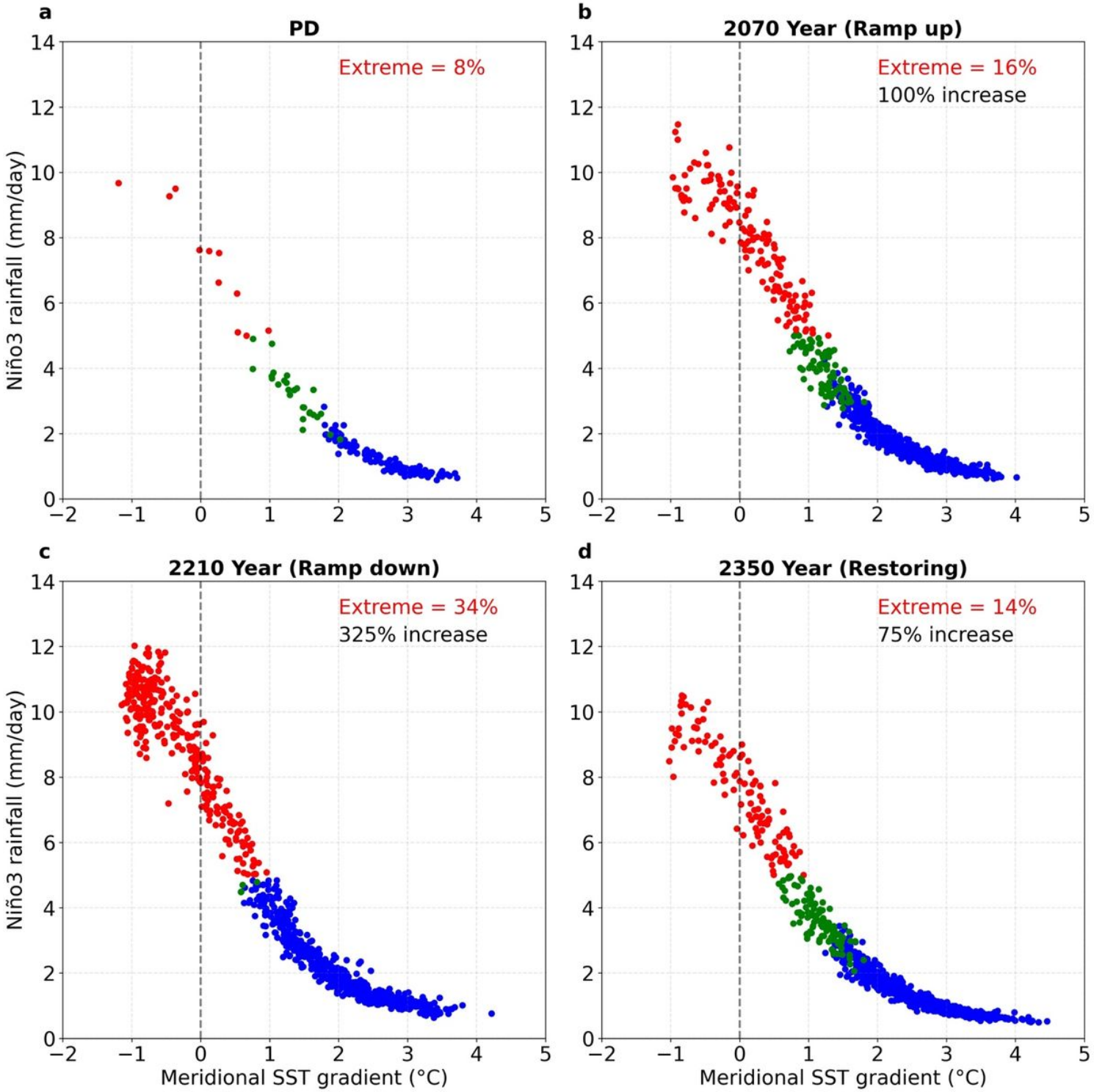

Figure 1

Nonlinear characteristics of model convective extreme El Niño (CEE) and changes in occurrences. Relationship between Niño3 (5° S-5° N, 150° W-90° W) boreal winter total rainfall and meridional SST gradient (average SST over the off-equatorial region (5° N-10° N, 150° W-90° W) minus the average over the equatorial region (2.5° S-2.5° N, 150° W-90° W)) for, **a)** present-day climate, **b)** ramp-up (Year 2070), **c)** ramp-down (Year 2210), and **d)** restoring (Year 2350). CEE (defined as events that exceed boreal winter rainfall of 5mm/day threshold), moderate El Niño (events with Niño3 SST anomalies greater than 0.5

standard deviation, but not CEE events), and La Niña and neutral events are denoted by red, green, and blue dots respectively. The percentage of occurrences of CEE events in each period is shown. The frequency change in CEE events in Year 2210 (compared to other periods) is significant at 99% confidence level.

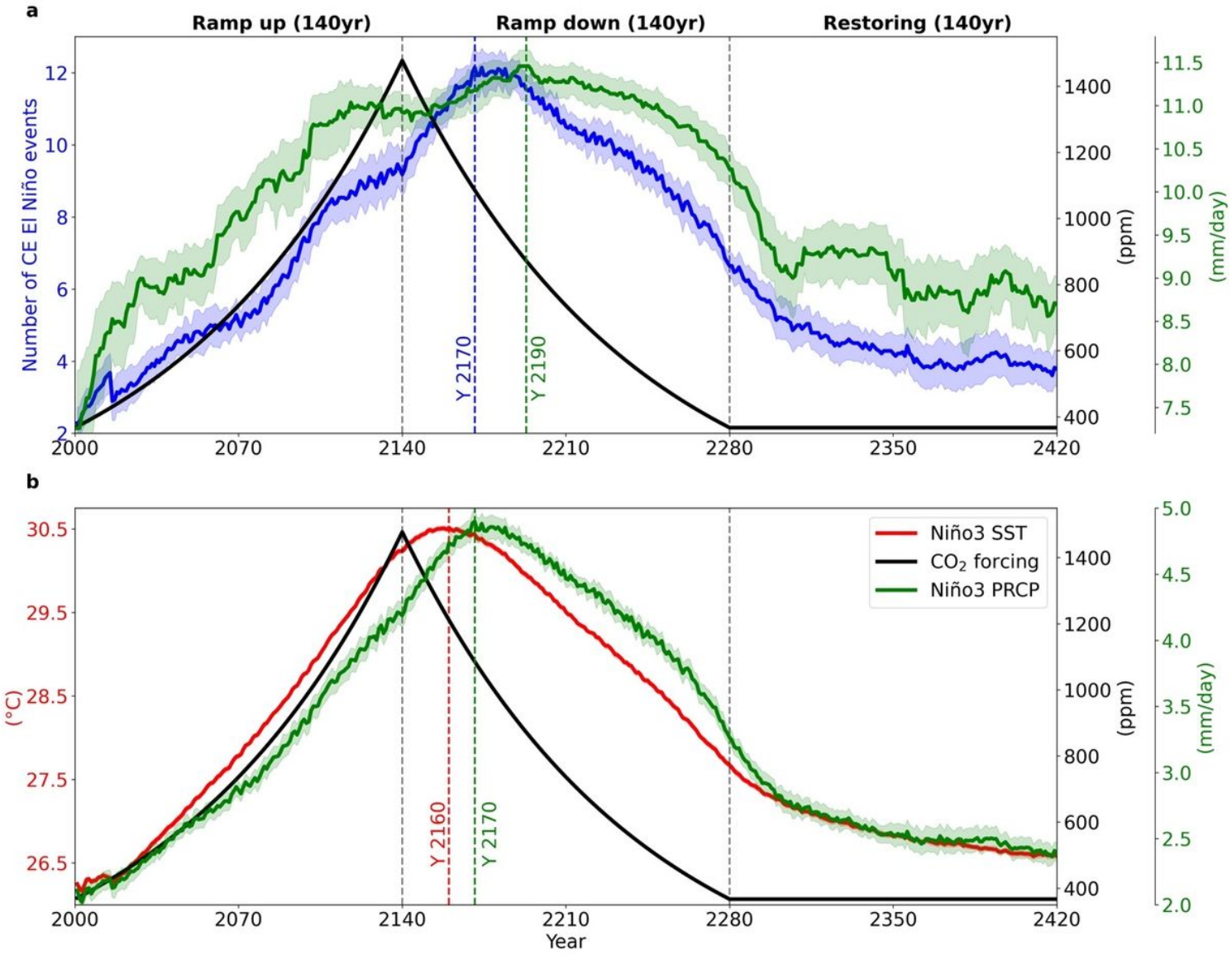

Figure 2

Evolution of convective extreme El Niño (CEE), Niño3 SST, and precipitation. Timeseries of **a)** CO_2 concentration (black line), Number of CEE (total cases per 31-years, blue line), precipitation of maximum CEE (green line), and **b)** Niño3 mean SST (red line), Niño3 mean precipitation (green line). The vertical lines indicate the maximum or minimum Year of each variable. The solid lines and the shadings denote the ensemble means and the 95% confidence level of the mean, respectively. All the variables except CO_2 have been smoothed using a 31-year running mean.

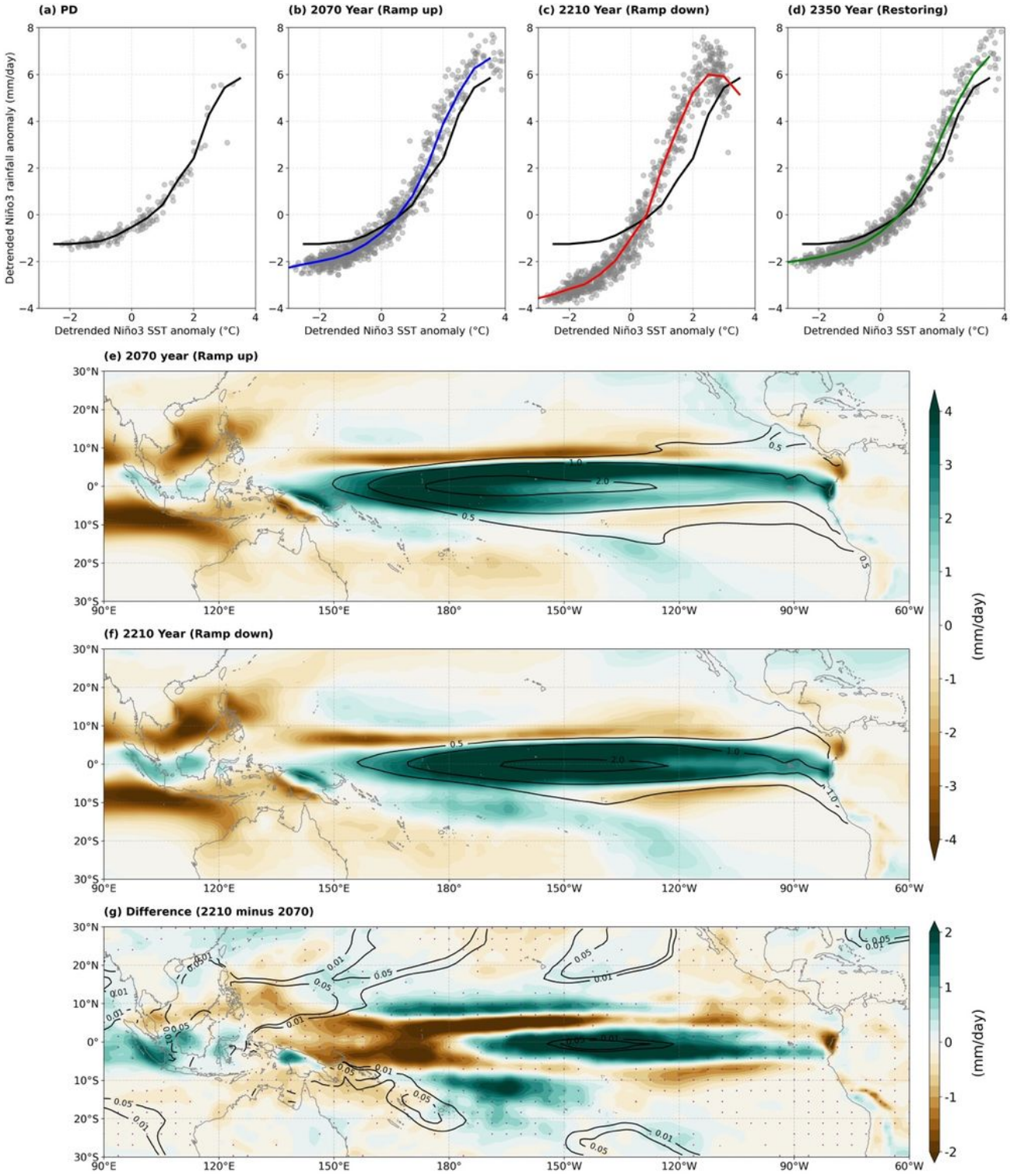

Figure 3

Changes in Niño3 SST-rainfall relationship. Scatter plot of detrended boreal winter Niño3 SST anomaly and rainfall anomaly for, **a)** present-day climate, **b)** ramp-up (Year 2070), **c)** ramp-down (Year 2210), and **d)** restoring (Year 2350). The black, blue, red, and green lines show the regression for the present, ramp-up, ramp-down, and restoring periods, respectively. Boreal winter SST (contours) and precipitation (shading) anomaly composite for Niño3 index between 1° C to 2° C is shown for **e)** ramp-up (Year 2070),

and **f)** ramp-down (Year 2210), and **g)** the difference of precipitation anomaly (Year 2210 minus Year 2070). The purple dots indicate the significant regions at 95% confidence level.

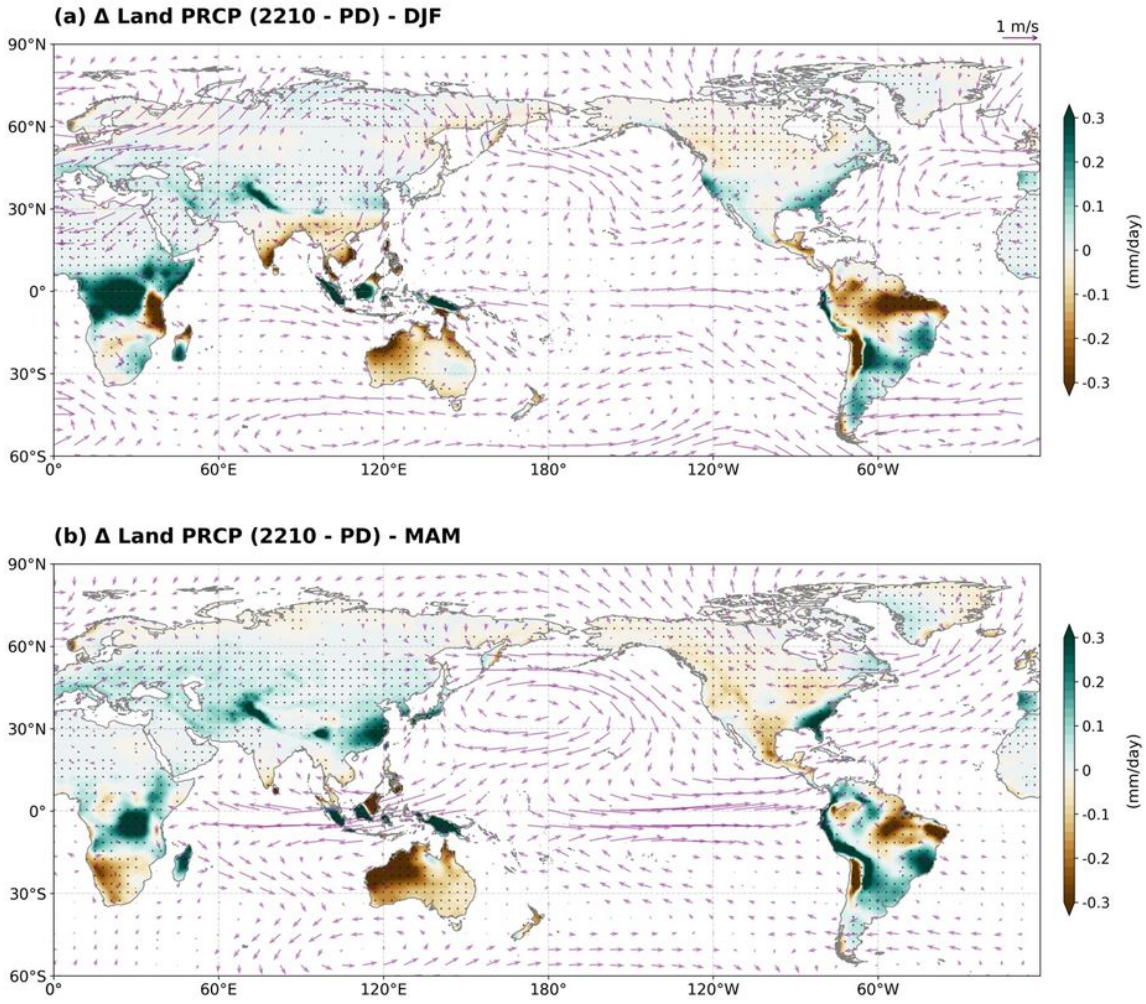

Figure 4

Changes in the land precipitation during CEE. Difference in the land precipitation anomalies (shading) and 850hPa winds (vector) for **a)** boreal winter, and **b)** following spring, between Year 2210 and PD climate. The regions marked with black dots denote the significant regions at the 95% confidence interval. Difference is calculated as the contribution to the mean-state change by CEE in Year 2210 (Supplementary Fig. 3d, see methods) minus the contribution to the mean-state change by CEE in PD (Supplementary Fig. 3c).

Supplementary Files

This is a list of supplementary files associated with this preprint. Click to download.

- CEEManuscriptsupplementary.pdf